Direct singular positions of the parallel manipulator Tricept

C H Liu* and **F-K Hsu**
Department of Mechanical and Electro-Mechanical Engineering, Tamkang University, Taipei Shien, Taiwan, Republic of China

The manuscript was received on 26 January 2006 and was accepted after revision for publication on 5 October 2006.

DOI: 10.1243/0954406JMES301

Abstract: In this article, the direct singular positions of the parallel manipulator Tricept are determined. An alternative 3×3 Jacobian matrix, simpler than the existing one, is obtained in this study. For a given moving platform's orientation, the determinant of this Jacobian matrix may be expressed as a cubic polynomial in moving platform's extension length. Direct singular positions may thus be obtained by solving cubic polynomial equations. For an arbitrarily chosen moving platform's orientation, there exists at least one moving platform's extension length that causes direct kinematic singularity. It is found that if moving platform's size is larger than a specific value, then within the moving platform's domain there exist two regions, in which direct kinematic singularities can only occur at positions impossible to reach.

Keywords: direct kinematic singularities, Tricept, parallel manipulators, parallel robots, kinematics of machinery

1 INTRODUCTION

Parallel manipulators have high stiffness and low inertia; hence, they can be used in high speed manufacturing processes. Machining instruments based on the architecture of six-degree-of-freedom (DOF) parallel manipulators have been developed [**1**, **2**]. Alternatively, manufacturing units may be formed by a limited DOF parallel manipulator in combination with a serial (or another parallel) manipulator, and such kinds of systems are called hybrid kinematic machines [**3**, **4**]. Figure 1 shows the schematic diagram of the hybrid kinematic machine Tricept [**5**, **6**], which consists of a three-DOF parallel manipulator and a serial manipulator with two or three DOFs. The three-DOF parallel manipulator has four limbs. The middle limb is passive and has only one link that connects the moving platform and the base with a prismatic (P) joint and a universal (U) joint, respectively. Other three limbs have the common SPS structure, i.e. two links are joined by a prismatic (P) pair, and this limb connects both the moving platform and the base by spherical (S) joints. The parallel manipulator is driven by three linear actuators in the three prismatic pairs of the SPS limbs. The middle limb is passive, which allows the moving platform to possess the following three-DOF motion: two rotations provided by the U joint and an extension provided by the P joint. Note that spinning of the moving platform about the longitudinal axis of the middle limb is restrained by both the U joint and the P joint of this limb. In what follows, the term Tricept is restricted to mean the three-DOF parallel manipulator only.

Tricept has been utilized in high-speed milling, drilling, welding, and deburring processes [**7**]. Many research efforts have been devoted to the analysis and design of this manipulator. Siciliano [**8**] suggested a numerical procedure for kinematic analysis and proved that convergence can always be obtained. Caccavale *et al.* [**9**] obtained kinematic and dynamic models for analyses and control. Zhang and Gosselin [**10**] established a kinetostatic model to analyse and optimize the stiffness properties of Tricept. Joshi and Tsai [**3**] performed a direct position analysis for Tricept. They obtained polynomial equations for moving platform positions and found that there are

Corresponding author: Department of Mechanical and Electro-Mechanical Engineering, Tamkang University, Tamsui, Taipei Shien 251, Taiwan, Republic of China. email: chaohwa@mail.tku.edu.tw

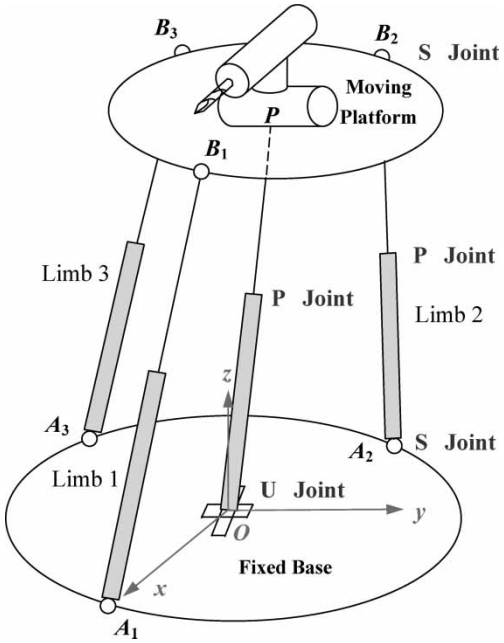

Fig. 1 An illustrative diagram of the hybrid kinematic machine – Tricept

at most 24 solutions in a direct position analysis. In comparing Tricept with the 3UPU parallel manipulator, Joshi and Tsai [**4**] found that Tricept has a larger workspace and also a much higher value in the minimum stiffness. In these aspects, Tricept is a better three-DOF parallel manipulator than the 3UPU manipulator.

It is known that kinematic singularity positions exist in the workspace of a parallel manipulator [**11**]. Kinematic singularity can be categorized into the following three types [**12**]: direct singularity, inverse singularity, and combined singularity. At a direct singularity position, the moving platform gains certain DOFs and may perform micromovements even when all actuators are stationary [**12**, **13**]. Inverse singularities, in general, occur at workspace boundary. At such a position, the moving platform loses some DOFs even when actuators are still moving. At a combined singular position, both the above-mentioned properties occur. Combined singularities represent uncertainty positions [**13**], and they only appear in manipulators with particular dimensions [**12**]. Because direct singular positions often appear in the inside of the workspace, locating direct singularity positions of a parallel manipulator is much more difficult than locating inverse singular positions. Various attempts have been suggested in locating direct singular positions of parallel manipulators. For the 3-3 Stewart–Gough parallel manipulator, for example, they can be located by using screw theory [**14**], by using the Grassmann geometry [**15**], by solving polynomial equations of global coordinates that have 16 to 32 terms [**16**–**19**], by a numerical technique [**20**], or by using analogous mechanisms [**21**].

At a direct singular position, the corresponding Jacobian matrix becomes singular [**13**]. Hence in locating these singular positions, generally, the Jacobian matrix for a particular manipulator is derived first, and then the positions that make the determinant zero are located. A Jacobian matrix of Tricept has been derived [**3**]. It is the multiplication of a 3×6 matrix by a 6×3 matrix, resulting in a fully occupied 3×3 matrix. The determinant of this matrix is very complicated; hence, direct singular positions have not yet been determined. In this study, a new Jacobian matrix with a simpler determinant is derived. This determinant is a function of moving platform's position, namely, the two rotation angles of the U joint and the extension length of the P joint in the middle limb (Fig. 1). By specifying the rotation angles of the U joint, the determinant reduces to a cubic polynomial of the extension length. Hence, direct singular positions can be determined by solving cubic equations [**13**, **21**]. Direct singular positions thus determined are substituted into the existing Jacobian matrix [**3**] to verify results.

2 JACOBIAN MATRIX

Three spherical joints A_1, A_2, A_3 on the fixed base form an equilateral triangle. The origin O of the xyz coordinate system is located at the circumcentre of this triangle (Fig. 2(a)). In this study, all lengths are normalized by the distance OA_1. In other words, all the manipulators analysed in this study have the base dimensions $OA_1 = OA_2 = OA_3 = A_{1x} = 1$. The three spherical joints B_1, B_2, B_3 on the moving platform also form an equilateral triangle, the circumcentre of which is denoted by P. The dimensions of this triangle, already normalized by OA_1, are given by the relation $PB_1 = PB_2 = PB_3 = b$ (Fig. 2(b)). The point P is also the origin of the body-fixed coordinate

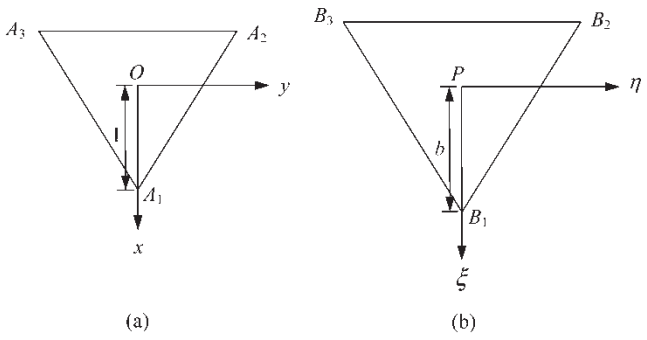

Fig. 2 The illustrative diagrams of the base and the moving platform: (a) fixed base and (b) moving platform

system denoted by (ξ, η, ζ). The ξ and η axes lie on the moving platform and are directed as shown in Fig. 2(b). The ζ axis is normal to the moving platform.

The moving platform of Tricept has an extended part that is connected to the middle limb by a prismatic joint (i.e. the part above the prismatic joint in Fig. 1 is fixed to the moving platform). Hence, the orientation of the moving platform can be determined by the direction of the vector ***OP***, which can be specified by two angles as explained below. In Fig. 3, the movable axes ξ–η–ζ originally coincide with the x, y, and z axes, respectively. To bring the ζ axis to coincide with ***OP***, one may first rotate the ξ–η–ζ frame about the x axis by an angle ϕ to move the ζ axis to pass through the point P', which is the projection of the point P onto the yz plane, as Fig. 3 shows. This rotation moves the ξ–η–ζ axes into the positions of ξ'–η'–ζ', as shown in Fig. 3. A second rotation about the η' axis by an angle θ carries the ζ axis into ***OP***. Orientation of ***OP*** is, therefore, specified by (ϕ, θ), which can be identified with the first two Bryant angles [**22**]. Without losing generality, values of ϕ and θ are confined to the ranges: $-\pi/2 \leqslant \phi \leqslant \pi/2$, $-\pi/2 \leqslant \theta \leqslant \pi/2$; meaning that the domain of (ϕ, θ) is a square region in the ϕ–θ plane. An arbitrary combination of ϕ and θ determines a unique orientation of the moving platform, although the same vector ***OP*** may correspond to more than one combination of (ϕ, θ). For example, the situation ***OP*** lies on the x axis can be obtained by simply setting $\theta = \pi/2$, leaving ϕ arbitrary, but each value of ϕ defines a specific orientation of the moving platform. If the normalized length of ***OP*** is denoted by r, then moving platform's position is uniquely determined by (ϕ, θ, r).

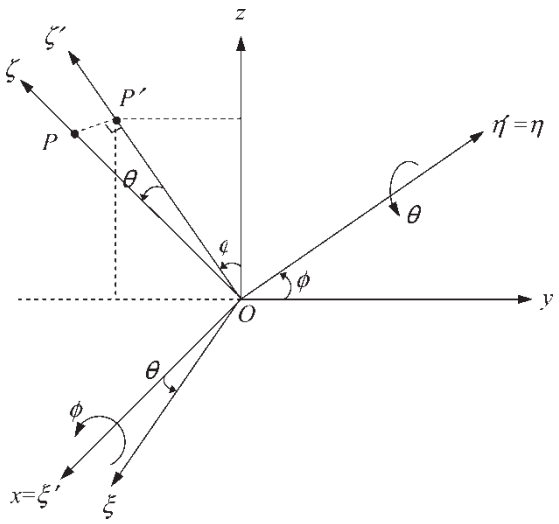

Fig. 3 The revolving angles of U joint

The direction cosine matrix **R** between the xyz frame and the $\xi\eta\zeta$ frame (Fig. 3) is given by

$$[\mathbf{R}] = \begin{bmatrix} 1 & 0 & 0 \\ 0 & \mathrm{c}\,\phi & -\mathrm{s}\,\phi \\ 0 & \mathrm{s}\,\phi & \mathrm{c}\,\phi \end{bmatrix} \begin{bmatrix} \mathrm{c}\,\theta & 0 & \mathrm{s}\,\theta \\ 0 & 1 & 0 \\ -\mathrm{s}\,\theta & 0 & \mathrm{c}\,\theta \end{bmatrix} = \begin{bmatrix} \mathrm{c}\,\theta & 0 & \mathrm{s}\,\theta \\ \mathrm{s}\,\phi\,\mathrm{s}\,\theta & \mathrm{c}\,\phi & -\mathrm{s}\,\phi\,\mathrm{c}\,\theta \\ -\mathrm{c}\,\phi\,\mathrm{s}\,\theta & \mathrm{s}\phi & \mathrm{c}\,\phi\,\mathrm{c}\,\theta \end{bmatrix} \tag{1}$$

where c and s denote cosine and sine functions, respectively. If ***OP*** has a length r, then the xyz coordinates of P are given by

$$\begin{Bmatrix} P_x \\ P_y \\ P_z \end{Bmatrix} = [\mathbf{R}] \begin{Bmatrix} 0 \\ 0 \\ r \end{Bmatrix} = \begin{Bmatrix} r\,\mathrm{s}\,\theta \\ -r\,\mathrm{s}\,\phi\,\mathrm{c}\,\theta \\ r\,\mathrm{c}\,\phi\,\mathrm{c}\,\theta \end{Bmatrix} \tag{2}$$

Coordinates of B_1, B_2, and B_3 in (ξ, η, ζ) coordinate system are (b, 0, 0), ($-b/2$, $\sqrt{3}$b/2, 0) and ($-b/2$, $-\sqrt{3}$b/2, 0), respectively. Their xyz coordinates are

$$\begin{Bmatrix} B_{1x} \\ B_{1y} \\ B_{1z} \end{Bmatrix} = \boldsymbol{OP} + \boldsymbol{PB_1} = \begin{Bmatrix} r\,\mathrm{s}\,\theta \\ -r\,\mathrm{s}\,\phi\,\mathrm{c}\,\theta \\ r\,\mathrm{c}\,\phi\,\mathrm{c}\,\theta \end{Bmatrix} + [\mathbf{R}] \begin{Bmatrix} b \\ 0 \\ 0 \end{Bmatrix} = \begin{Bmatrix} r\,\mathrm{s}\,\theta + b\,\mathrm{c}\,\theta \\ -r\,\mathrm{s}\,\phi\,\mathrm{c}\,\theta + b\,\mathrm{s}\,\phi\,\mathrm{s}\,\theta \\ r\,\mathrm{c}\,\phi\,\mathrm{c}\,\theta - b\,\mathrm{c}\,\phi\,\mathrm{s}\,\theta \end{Bmatrix} \tag{3a}$$

$$\begin{Bmatrix} B_{2x} \\ B_{2y} \\ B_{2z} \end{Bmatrix} = \begin{Bmatrix} r\,\mathrm{s}\,\theta - (b\,\mathrm{c}\,\theta)/2 \\ -r\,\mathrm{s}\,\phi\,\mathrm{c}\,\theta - (b\,\mathrm{s}\,\phi\,\mathrm{s}\,\theta)/2 + (\sqrt{3}b\,\mathrm{c}\,\phi)/2 \\ r\,\mathrm{c}\,\phi\,\mathrm{c}\,\theta + (b\,\mathrm{c}\,\phi\,\mathrm{s}\,\theta)/2 + (\sqrt{3}b\,\mathrm{s}\,\phi)/2 \end{Bmatrix} \tag{3b}$$

$$\begin{Bmatrix} B_{3x} \\ B_{3y} \\ B_{3z} \end{Bmatrix} = \begin{Bmatrix} r\,\mathrm{s}\,\theta - (b\,\mathrm{c}\,\theta)/2 \\ -r\,\mathrm{s}\,\phi\,\mathrm{c}\,\theta - (b\,\mathrm{s}\,\phi\,\mathrm{s}\,\theta)/2 - (\sqrt{3}b\,\mathrm{c}\,\phi)/2 \\ r\,\mathrm{c}\,\phi\,\mathrm{c}\,\theta + (b\,\mathrm{c}\,\phi\,\mathrm{s}\,\theta)/2 - (\sqrt{3}b\,\mathrm{s}\,\phi)/2 \end{Bmatrix} \tag{3c}$$

The xyz coordinates of A_1, A_2, and A_3 are (1, 0, 0), ($-1/2$, $-\sqrt{3}/2$, 0), and ($-1/2$, $-\sqrt{3}/2$, 0). Using these coordinates, one may show that limb lengths A_iB_i ($i = 1, 2, 3$), denoted by d_i, satisfy the following

relations [**23**]

$$d_1^2 = (r\,\mathrm{s}\,\theta + b\,\mathrm{c}\,\theta - 1)^2 + (-r\,\mathrm{s}\,\phi\,\mathrm{c}\,\theta + b\,\mathrm{s}\,\phi\,\mathrm{s}\,\theta)^2 + (r\,\mathrm{c}\,\phi\,\mathrm{c}\,\theta - b\,\mathrm{c}\,\phi\,\mathrm{s}\,\theta)^2 \quad (4a)$$

$$d_2^2 = \frac{1}{4}\Big[(2r\,\mathrm{s}\,\theta - b\,\mathrm{c}\,\theta + 1)^2 + (\sqrt{3}b\,\mathrm{c}\,\phi - 2r\,\mathrm{s}\,\phi\,\mathrm{c}\,\theta - b\,\mathrm{s}\,\phi\,\mathrm{s}\,\theta - \sqrt{3})^2 + (2r\,\mathrm{c}\,\phi\,\mathrm{c}\,\theta + b\,\mathrm{c}\,\phi\,\mathrm{s}\,\theta + \sqrt{3}b\,\mathrm{s}\,\phi)^2\Big] \quad (4b)$$

$$d_3^2 = \frac{1}{4}\Big[(2r\,\mathrm{s}\,\theta - b\,\mathrm{c}\,\theta + 1)^2 + (-\sqrt{3}b\,\mathrm{c}\,\phi - 2r\,\mathrm{s}\,\phi\,\mathrm{c}\,\theta - b\,\mathrm{s}\,\phi\,\mathrm{s}\,\theta + \sqrt{3})^2 + (2r\,\mathrm{c}\,\phi\,\mathrm{c}\,\theta + b\,\mathrm{c}\,\phi\,\mathrm{s}\,\theta - \sqrt{3}b\,\mathrm{s}\,\phi)^2\Big] \quad (4c)$$

Direct kinematic singularity means that the moving platform can perform micromovements even when all drivers are locked, that is, when $\dot{d}_1 = \dot{d}_2 = \dot{d}_3 = 0$. Using equations (4a) to (c) to obtain $\dot{d}_i$, and letting $\dot{d}_i = 0$, one may obtain [**23**]

$$\mathbf{C}(\phi, \theta, r)\begin{bmatrix}\dot{\phi} & \dot{\theta} & \dot{r}\end{bmatrix}^{\mathrm{T}} = \mathbf{0} \quad (5)$$

where $\mathbf{C}$ is the 3×3 Jacobian matrix, whose elements are given below

$$C_{11} = 0 \quad (6a)$$

$$C_{12} = 2(b\,\mathrm{s}\,\theta - r\,\mathrm{c}\,\theta) \quad (6b)$$

$$C_{13} = 2(r - \mathrm{s}\,\theta) \quad (6c)$$

$$C_{21} = \frac{3}{2}b\,\mathrm{s}\,\phi + \frac{\sqrt{3}}{2}(2r\,\mathrm{c}\,\theta + b\,\mathrm{s}\,\theta)\mathrm{c}\,\phi \quad (6d)$$

$$C_{22} = \left(\frac{b}{2} - \sqrt{3}r\,\mathrm{s}\,\phi\right)\mathrm{s}\,\theta + \left(\frac{\sqrt{3}}{2}b\,\mathrm{s}\,\phi + r\right)\mathrm{c}\,\theta \quad (6e)$$

$$C_{23} = 2r + \mathrm{s}\,\theta + \sqrt{3}s\,\phi\,\mathrm{c}\,\theta \quad (6f)$$

$$C_{31} = \frac{3}{2}b\,\mathrm{s}\,\phi - \frac{\sqrt{3}}{2}(2r\,\mathrm{c}\,\theta + b\,\mathrm{s}\,\theta)\mathrm{c}\,\phi \quad (6g)$$

$$C_{32} = \left(\frac{b}{2} + \sqrt{3}\,r\,\mathrm{s}\,\phi\right)\mathrm{s}\,\theta - \left(\frac{\sqrt{3}}{2}b\,\mathrm{s}\,\phi - r\right)\mathrm{c}\,\theta \quad (6h)$$

$$C_{33} = 2r + s\,\theta - \sqrt{3}\mathrm{s}\,\phi\,\mathrm{c}\,\theta \quad (6i)$$

At a position that makes the determinant $|\mathbf{C}|$ zero, the moving platform may have a non-zero velocity vector $[\dot{\phi}\ \dot{\theta}\ \dot{r}]^{\mathrm{T}}$ when all drivers are locked. The purpose of this study is to locate all such positions.

3 DIRECT SINGULAR POSITIONS

The determinant of the Jacobian matrix $\mathbf{C}$ is

$$|\mathbf{C}| = C_{13}C_{21}C_{32} + C_{12}C_{23}C_{31} - C_{13}C_{22}C_{31} - C_{12}C_{21}C_{33} \quad (7)$$

Substituting equations (6a) to (i) into equation (7) and forcing the determinant to be zero, the following cubic equation of r be obtained [**23**]

$$\Omega_1 r^3 + \Omega_2 r^2 + \Omega_3 r + \Omega_4 = 0 \quad (8)$$

where coefficients Ω_i ($i = 1, 2, 3$) depend on ϕ and θ, as follows

$$\Omega_1 = 12\mathrm{c}\,\phi\,\mathrm{c}^2\theta \quad (9a)$$

$$\Omega_2 = 6b\mathrm{s}^2\,\phi\,\mathrm{s}\,\theta \quad (9b)$$

$$\Omega_3 = -3b^2\,\mathrm{c}\,\phi\,\mathrm{s}^2\theta - 3b^2\mathrm{s}^2\,\phi\,\mathrm{c}\,\theta - 6b\,\mathrm{c}\,\phi\,\mathrm{s}^2\theta\,\mathrm{c}\,\theta - 6b\,\mathrm{s}^2\phi \quad (9c)$$

$$\Omega_4 = 3b^2(3\mathrm{s}^2\,\phi\,\mathrm{c}\,\theta - \mathrm{c}\,\phi\,\mathrm{s}^2\theta)\mathrm{s}\,\theta \quad (9d)$$

If the coefficient $\Omega_1 \neq 0$, then the three roots are given by [**24**]

$$r_1 = S + T - \frac{\Omega_2}{3\Omega_1} \quad (10a)$$

$$r_2 = -\frac{S+T}{2} - \frac{\Omega_2}{3\Omega_1} + \frac{1}{2}i\sqrt{3}(S - T) \quad (10b)$$

$$r_3 = -\frac{S+T}{2} - \frac{\Omega_2}{3\Omega_1} - \frac{1}{2}i\sqrt{3}(S - T) \quad (10c)$$

where

$$S = \sqrt[3]{R + \sqrt{Q^3 + R^2}} \quad (11a)$$

$$T = \sqrt[3]{R - \sqrt{Q^3 + R^2}} \quad (11b)$$

$$Q = \frac{3\Omega_3\Omega_1 - \Omega_2^2}{9\Omega_1^2} \quad (11c)$$

$$R = \frac{9\Omega_1\Omega_2\Omega_3 - 27\Omega_4\Omega_1^2 - 2\Omega_2^3}{54\Omega_1^3} \quad (11d)$$

A cubic polynomial equation has at least one real root. For values of ϕ and θ arbitrarily chosen from the domain $-\pi/2 \leqslant \phi,\ \theta \leqslant \pi/2$, there exists at least one extension length r that gives rise to direct singularity. After such a length r is obtained, the corresponding spherical joint positions can be found by using equations (3a) to (c). The direct singular positions thus determined are substituted into the Jacobian matrix obtained from reference [**3**] to

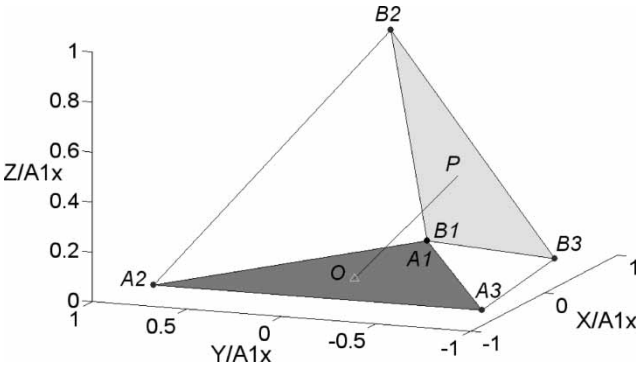

Fig. 4 Direct singular position for the case $\phi = \theta = \pi/4$ and $b = r = 1/\sqrt{2}$

verify the results. A MATLAB program is written to perform the above-mentioned numerical calculations and also to generate graphical outputs.

4 RESULTS AND DISCUSSIONS

Three obvious cases of direct singularity are discussed first. The first case is when the normalized lengths b and r take the following values: $b = \cos\theta$ and $r = \sin\theta$ $(0 \leqslant \theta \leqslant \pi/2)$. Substituting these values into equations (6b) and (6c), one may find that $C_{12} = C_{13} = 0$. Matrix **C** is singular because all elements in the first row are zero. By using equation (4a), one may also show that the first limb length d_1 is always zero in this case. A particular configuration when $b = r = 1/\sqrt{2}$ (i.e. $\phi = \theta = \pi/4$) is shown in Fig. 4. The second obvious case is when $\phi = 0$ and $r = -(b \tan\theta)/2$ and θ is confined to the region $-\pi/2 \leqslant \theta \leqslant 0$. It can be seen from equations (6d) to (g) that $C_{21} = C_{31} = 0$. Hence, all elements in the first column of **C** are zero. Figure 5 shows the singular configuration when $(\phi, \theta) = (0, -\pi/4)$, $b = 2$, and $r = 1$. It can be seen from this figure that two limbs lie on the base plane in this particular singular position. The third case is obtained by setting

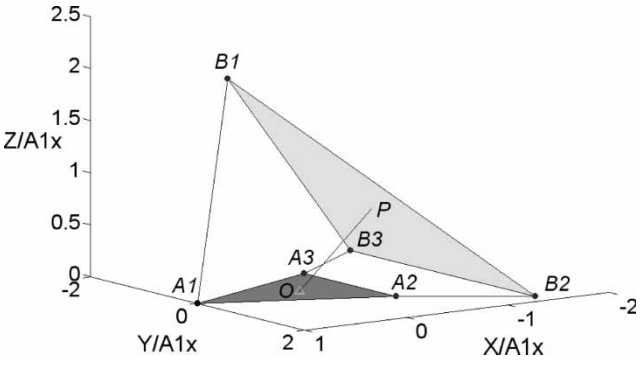

Fig. 5 Direct singular position for the case $(\phi, \theta) = (0, -\pi/4)$, $b = 2$, and $r = 1$

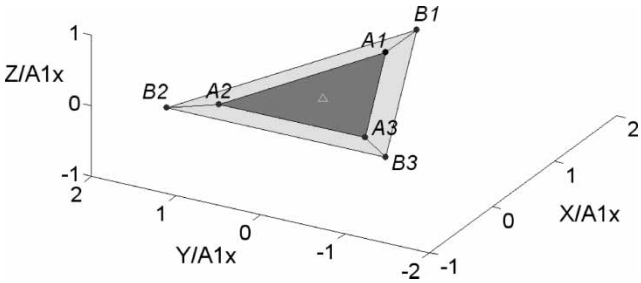

Fig. 6 Direct singular position for the case $(\phi, \theta) = (0, 0)$, $b = 1.5$, and $r = 0$

$\phi = \theta = 0$ in equations (9c) to (d), coefficients $\Omega_2 = \Omega_3 = \Omega_4 = 0$ in this case. Equation (8) reduces to the form $\Omega_1 r^3 = 0$, and it has a triple root at $r = 0$. The corresponding configuration is shown in Fig. 6, from which it is seen the moving platform coincides with the base.

Although the forgoing cases were obtained by observation, all the following singular positions are obtained by first choosing ϕ and θ values from the domain $[-\pi/2, \pi/2]$ and then solving equation (8) to obtain the extension length r. It can be easily seen that all the coefficients Ω_i $(i = 1, 2, 3, 4)$ remain the same if ϕ is replaced by $-\phi$ and that only Ω_2 and Ω_4 change sign if θ is replaced by $-\theta$. This means that solutions to equation (8) are symmetric about the line $\phi = 0$ and anti-symmetric about the line $\theta = 0$. In other words, if direct singularity appears at (ϕ, θ, r), then it also appears at $(-\phi, \theta, r)$, $(\phi, -\theta, -r)$, and $(-\phi, -\theta, -r)$. In the following discussions, the three real roots to equation (8), denoted by r_1, r_2, and r_3, are arranged in the descending order of absolute values, namely, $|r_1| \geqslant |r_2| \geqslant |r_3|$. Figures 7 to 9 show the three singular surfaces in the three-dimensional (ϕ, θ, r) space. These singular positions can be classified into the following three categories.

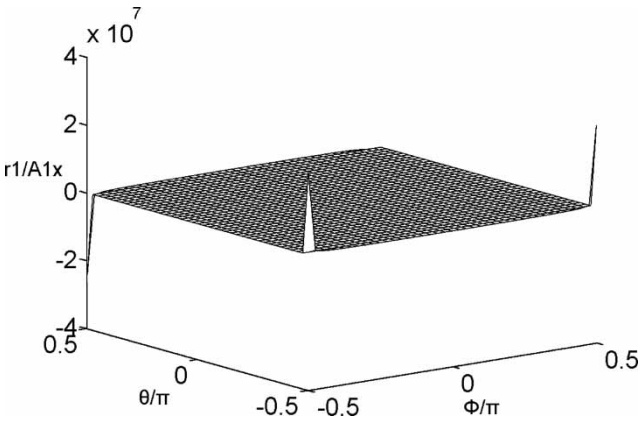

Fig. 7 The singular surface generated by root r_1

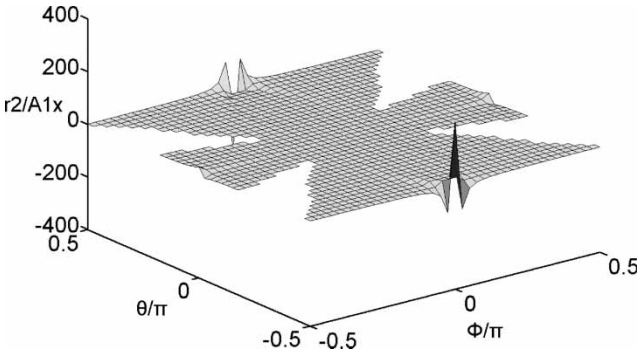

Fig. 8 The singular surface generated by root r_2

1. $\Omega_1 \neq 0$: then either one or three real roots exist. All points lie inside the square domain for (ϕ, θ) to fall into this category. Figure 7 shows that a real root r_1 always exists, but Figs 8 and 9 show that the second and the third real roots r_2 and r_3 do not exist in some regions. For the particular case (ϕ, θ) = (0.518, 0.108), there are three real roots: $r_1 = -0.6919$, $r_2 = 0.5300$, and $r_3 = 0.1389$. The corresponding three singular configurations are shown in Fig. 10. The moving platform in these configurations is parallel, because they have the same values of ϕ and θ.
2. $\Omega_1 = 0$ but $\Omega_2 \neq 0$: from equation (9a), one knows that $\Omega_1 = 0$ when $\phi = \pm\pi/2$ or $\theta = \pm\pi/2$. Hence, all points on the boundary of the square region cause degeneracy of the cubic equation. If $\Omega_2 \neq 0$, the equation becomes quadratic. In such a case, no real root exists when $\Omega_3^2 - 4\Omega_2\Omega_4 < 0$. The authors found that along the boundaries $\phi = \pm\pi/2$, no real root exists in the two intervals: $-1.4682 \leqslant \theta \leqslant -0.6193$ and $0.6193 \leqslant \theta \leqslant 1.4682$. Also, as ($\phi$, θ) approaches the four corner points ($\pm\pi/2$, $\pm\pi/2$), the coefficient Ω_1 is of the order of 0^3, hence it approaches to zero very rapidly, making the root r_1 approach infinity (equations (10a) to (c)), as Fig. 7 shows.

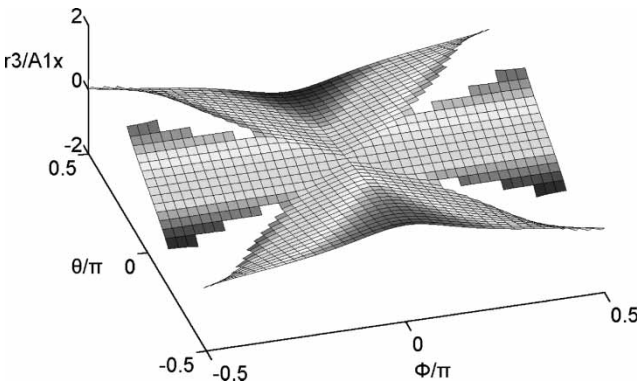

Fig. 9 The singular surface generated by root r_3

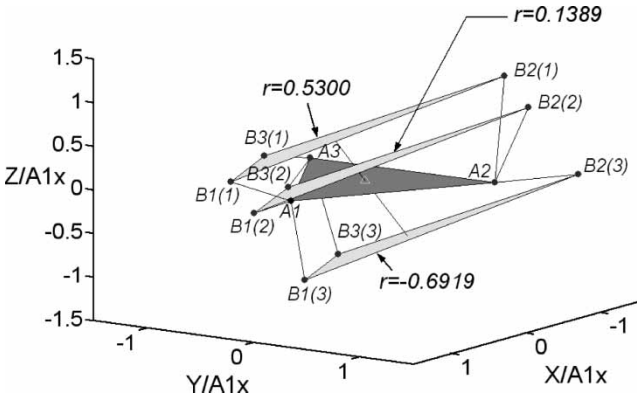

Fig. 10 Direct singular position for the case (ϕ, θ) = (0.5180, 0.1080), $b = 1.5$, $r = 0.5300$, 0.1389, and -0.6919

3. $\Omega_1 = \Omega_2 = 0$: equation (8) becomes linear. This happens in the following two cases: (a) $\cos\phi = \sin\theta = 0$, that is, ($\phi$, θ) = ($\pm\pi/2$, 0) and (b) $\sin\phi = \cos\theta = 0$, which means that ($\phi$, θ) = (0, $\pm\pi/2$). In the former case (i.e. $\cos\phi = \sin\theta = 0$), Ω_4 is zero, and the root $r = 0$ is obtained. The direct singular configurations for (ϕ, θ) = ($-\pi/2$, 0) and (ϕ, θ) = ($\pi/2$, 0) are shown in Figs 11 and 12, respectively. It can be noticed that the moving platforms are orthogonal to the base. In the latter case (i.e. $\sin\phi = \cos\theta = 0$), then $\Omega_3 = \pm\Omega_4$, hence $r = \pm 1$. Singular configurations shown in Figs 13 and 14 are for cases with (ϕ, θ) = (0, $-\pi/2$) and (ϕ, θ) = (0, $\pi/2$), respectively, again the moving platforms are normal to the base.

In the current numerical procedure, whenever a direct singular position is determined, it is introduced into the Jacobian matrix found in reference [**3**].

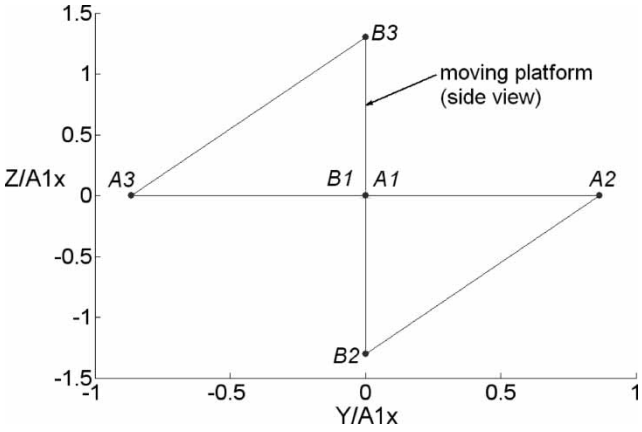

Fig. 11 Direct singular position for the case (ϕ, θ) = ($-\pi/2$, 0), $b = 1.5$, and $r = 0$

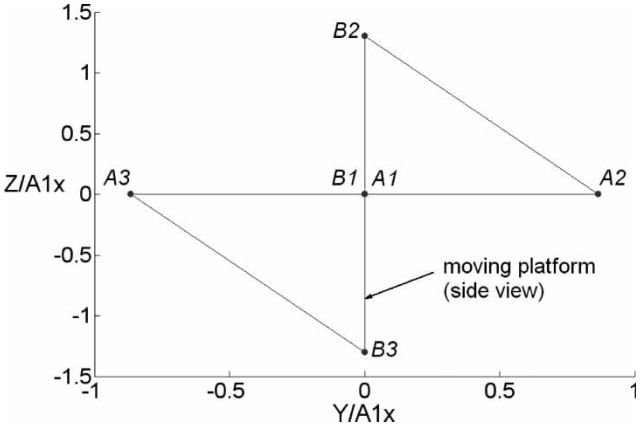

Fig. 12 Direct singular position for the case $(\phi, \theta) = (\pi/2, 0)$, $b = 1.5$, and $r = 0$

The configurations shown in Figs 4 to 6, 10 to 14 as well as the configurations corresponding to all the roots shown in Figs 7 to 9 are found to make the Jacobian matrix in reference [**3**] singular.

Inasmuch as the normalized extension r is expected to be non-negative, only non-negative roots are shown in Fig. 15. One may notice that there are two regions in which non-negative values of r do not exist; hence, in practice, direct kinematic singularities do not occur in these regions. Figure 15 is valid for the particular moving platform size $b = 1.5$, and the purpose of the following analysis is to determine whether such regions also exist for other values of b. According to Descartes' rule of sign, the number of positive real roots of equation (8) is equal to the number of sign changes of its coefficients Ω_i or is less than that number by 2. The number of negative roots may also be determined after replacing r by $(-r)$ in equation (8). Table 1 shows the signs of Ω_i and the numbers of positive/negative roots obtained by using Descartes' rule. In this table, the results for negative roots are shown

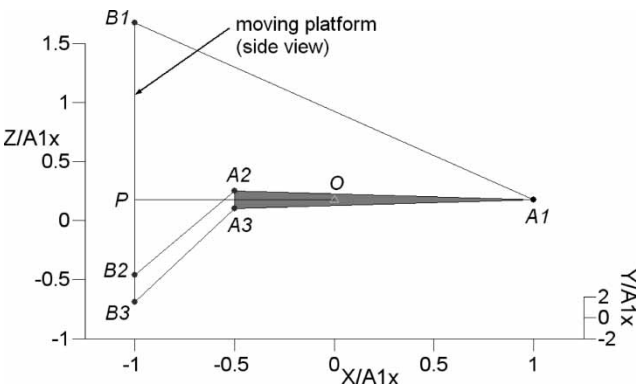

Fig. 13 Direct singular position for the case $(\phi, \theta) = (0, -\pi/2)$, $b = 1.5$, and $r = 1$

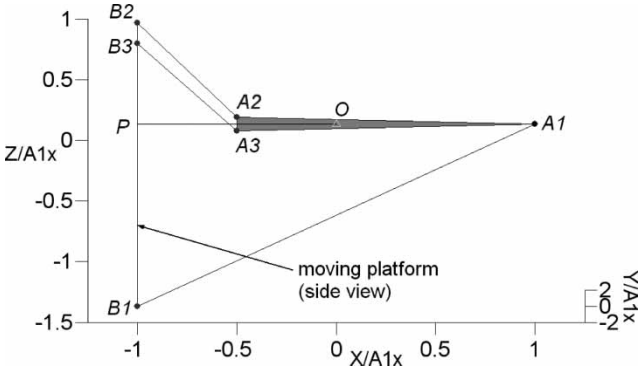

Fig. 14 Direct singular position for the case $(\phi, \theta) = (0, \pi/2)$, $b = 1.5$, and $r = -1$

in parentheses, and the variable Δ is defined by

$$\Delta = 3s^2\phi\, c\quad \theta - c\,\phi s^2\theta \tag{12}$$

Table 1 suggests that in either of the following two situations, there may be no positive real root:

(a) $\theta > 0$ and $\Delta > 0$;
(b) $\theta < 0$ and $\Delta < 0$.

Figure 16 shows two solid curves, and the points on which satisfy the equation $\Delta = 0$. These two curves, together with the line $\theta = 0$, separate the domain into several regions. Both the two regions satisfying $\theta > 0$ and $\Delta > 0$ are labelled as region 1, and the region satisfying $\theta < 0$ and $\Delta < 0$ is region 2. One knows from Table 1 that equation (8) has a negative real root for any point in regions 1 and 2. Hence, the appearance of two complex roots can rule out the possibility of a positive real root. As the coefficient $\Omega_1 \neq 0$, two complex roots for equation (8) may appear when the variables Q and R defined by equations (11c) and (d) satisfy the inequality

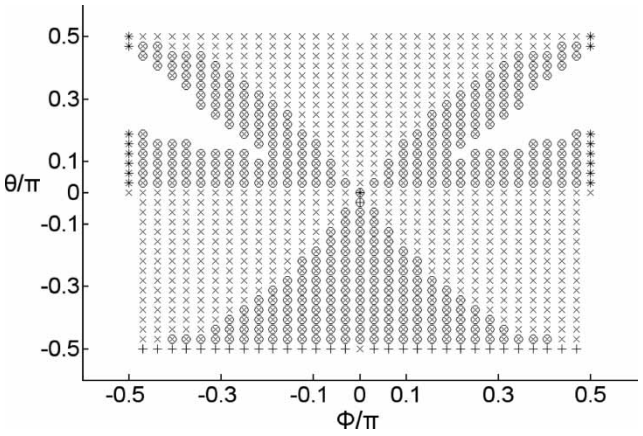

Fig. 15 Direct singular positions with non-negative roots ($r \geqslant 0$), $b = 1.5$, three roots r_1, r_2, and r_3 are denoted by x, +, and o, respectively

Table 1 Number of positive and negative roots of equation (8) according to Descartes' rule

				Ω_4		Sign change		Positive roots (negative roots)	
	Ω_1	Ω_2	Ω_3	$\Delta > 0$	$\Delta < 0$	$\Delta > 0$	$\Delta < 0$	$\Delta > 0$	$\Delta < 0$
$\theta > 0$	+ (−)	+ (+)	− (+)	+ (+)	− (−)	2 (1)	1 (2)	2 or 0 (1)	1 (2 or 0)
$\theta < 0$	+ (−)	− (−)	− (+)	− (−)	+ (+)	1 (2)	2 (1)	1 (2 or 0)	2 or 0 (1)

Δ is defined by equation (12), and numbers in parentheses are obtained when r is replaced by $(-r)$ in equation (8).

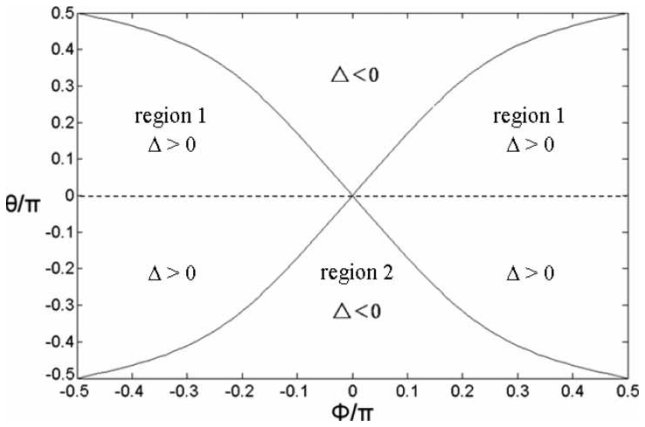

Fig. 16 Regions with positive/negative values of Δ: on solid lines $\Delta = 0$, the dashed line is $\theta = 0$

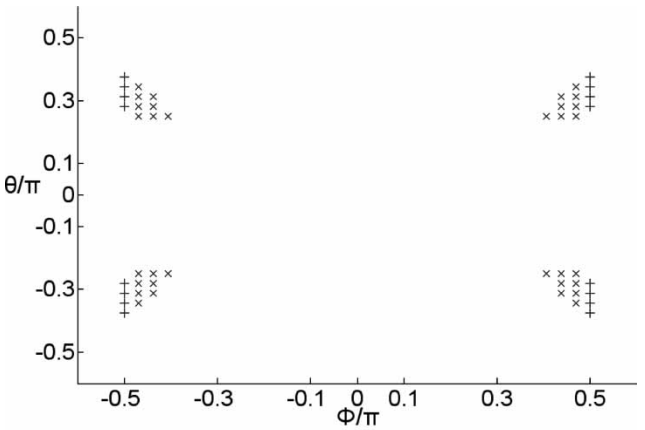

Fig. 17 Regions in which equation (8) has two complex roots, $b = 0.75$; $\times$ denotes points make $Q^3 + R^2 > 0$ and + denotes points make $\Omega_3^2 - 4\Omega_2\Omega_4 < 0$

$Q^3 + R^2 > 0$ [**24**]. However, if $\phi = \pm\pi/2$, Ω_1 becomes zero and equation (8) reduces to a quadratic equation. In this case, two complex roots may still appear if the discriminant $\Omega_3^2 - 4\Omega_2\Omega_4 < 0$. All the regions in which equation (8) has two complex roots, for the particular moving platform size $b = 0.75$, are shown in Fig. 17. A positive real root cannot exist within the intersections of regions shown in Fig. 17 and regions 1 and 2 in Fig. 16. For this reason, only the two upper regions shown in Fig. 17 do not contain any positive real root; meaning direct kinematic singularities cannot happen in these two regions in practice. The authors found that the size of the regions that have no direct singularity decreases with the moving platform size b. This can also be seen by comparing the size of the regions when $b = 1.5$, as shown in Fig. 15, with the size of the regions when $b = 0.75$, which are the two upper regions in Fig. 17. As the moving platform size b equals to 0.5824, the regions with no direct singularity reduce to the following two points $(\phi, \theta) = (\pm\pi/2, 0.33\pi)$. The regions vanish with a further decrease in the moving platform size.

5 CONCLUSIONS

In this study, a simpler Jacobian matrix for Tricept is obtained. By using this matrix, the direct kinematic singularity positions of Tricept and the corresponding configurations may be obtained by solving a cubic polynomial equation. The singular surfaces in the three-dimensional (ϕ, θ, r) space are shown. When the normalized moving platform size $b \geqslant 0.5824$, there are two regions in the ϕ–θ domain inside which direct kinematic singularities can only occur with impossible configurations. The size of these regions decreases with decreasing moving platform size b.

ACKNOWLEDGEMENT

The authors gratefully acknowledge that this study was partially supported by the National Science Council of ROC under grant no. NSC 93-2212-E032-015.

REFERENCES

1 **Giddings** and **Lewis.** Available from http://www.giddings.com.
2 **Toyoda Machine Works.** Available from http://www.toyoda-kouki.co.jp.
3 **Joshi, S.** and **Tsai, L. W.** A comparison study of two 3-DOF parallel manipulators: one with three and the

other with four supporting legs. *IEEE Trans. Robot. Autom.*, 2003, **19**(2), 200–209.
4 **Joshi, S.** and **Tsai, L. W.** The kinematics of a class of 3-DOF, 4-legged parallel manipulators. *ASME J. Mech. Des.*, 2003, **125**, 52–60.
5 **Comau**, available from http://www.comau.com.
6 **Neos Robotics**, available from http://www.neosrobotics.com.
7 **Neumann, K. E.** Tricept application. Proceedings of the 3rd Chemnitz Parallel Kinematics Seminar, Zwickau, Germany, 2002, pp. 547–551.
8 **Siciliano, B.** The Tricept robot: inverse kinematics, manipulability analysis and closed-loop direct kinematics algorithm. *Robotica*, 1999, **17**, 437–445.
9 **Caccavale, F., Siciliano, B.,** and **Villani, L.** The Tricept robot: dynamics and impedance control. *IEEE/ASME Trans. Mech.*, 2003, **8**(2), 263–268.
10 **Zhang, D.** and **Gosselin, C. M.** Kinetostatic analysis and design optimization of the tricept machine tool family. *J. Manuf. Sci. Eng.*, 2002, **124**, 725–733.
11 **Gosselin, C.** and **Angeles, J.** Singularity analysis of closed-loop kinematic chains. *IEEE Trans. Robot. Autom.*, 1990, **6**, 281–290.
12 **Tsai, L.-W.** *Robot analysis: the mechanics of serial and parallel manipulators*, 1999 (John Wiley & Sons, Inc., New York).
13 **Liu, C. H.** and **Cheng, S.** Direct singular positions of 3RPS parallel manipulators. *ASME J. Mech. Des.*, 2004, **126**, 1006–1016.
14 **Hunt, K. H.** *Kinematic geometry of mechanisms*, 1978 (Oxford University Press, Oxford, UK).
15 **Merlet, J. P.** Singular configurations of parallel manipulators and Grassmann Geometry. *Int. J. Robot. Res.*, 1989, **8**(5), 45–56.
16 **St-Onge, B. M.** and **Gosselin, C. M.** Singularity analysis and representation of spatial six-DOF parallel manipulators. *Recent advances in robot kinematics*, 1996, pp. 389–398 (Kluwer Academic Publishers, the Netherlands).
17 **Kim, D., Chung, W.,** and **Youm, Y.** Analytic singularity expression for 6-DOF Stewart platform-type parallel manipulator. Proceedings of the 1998 IEEE/RSJ International Conference on *Intelligent robots and systems*, Victoria, Canada, Oct. 13–17, 1998, pp. 1015–1019.
18 **St-Onge, B. M.** and **Gosselin, C. M.** Singularity analysis and representation of the general Gough–Stewart platform. *Int. J. Robot. Res.*, 2000, **19**(3), 271–288.
19 **Wang, J.** and **Gosselin, C. M.** Kinematic analysis and design of kinematically redundant parallel mechanisms. *J. Mech. Des.*, 2004, **126**, 109–118.
20 **Merlet, J. P.** *Parallel robots*, 2000. (Kluwer Academic Publishers, The Netherlands).
21 **Liu, C. H.** and **Chiu, J.** Direct kinematic singularities of 3-3 Stewart–Gough Platforms. *Proc. in IMechE, Part k: J. Multibody Dynamics*, 2005, **219**, 311–324.
22 **Nikravesh, P. E.** *Computer-aided analysis of mechanical systems*, 1988 (Prentice-Hall International, Eaglewood Cliffs).
23 **Hsu, F. K.** *Direct singular positions of the Tricept robot (in Chinese)*. Master Thesis, Department of Mechanical Engineering, Tamkang University, 2005.
24 **Spiegel, M. R.** and **Liu, J.** *Mathematic handbook of formulas and tables*, 2nd edition, 1999 (McGraw-Hill, NY).